Dynamics of the density of quantized vortex lines in counterflow turbulence: Experimental investigation

E. Varga and L. Skrbek
Faculty of Mathematics and Physics, Charles University, Ke Karlovu 3, 121 16, Prague 2, Czech Republic

(Received 6 December 2017; published 12 February 2018)

Recently the interest in thermal counterflow of superfluid ^{4}He, the most extensively studied form of quantum turbulence, has been renewed. Particularly, an intense theoretical debate has arisen about what form, if any, of the so-called Vinen equation accurately captures the dynamics of vortex line density, L. We address this problem experimentally, in a 21 cm long channel of square 7×7 mm^2 cross section. Based on large statistics of second-sound data measured in nonequilibrium square-wave modulated thermally induced counterflow we investigate the phase portrait of the general form of the governing dynamical equation and conclude that for sparse tangles ($L \lesssim 10^5$ cm^{-2}) all proposed forms of this equation based on the concept of a homogeneous random tangle of quantized vortices provide equally adequate descriptions of the growth of L, while for dense tangles ($L > 10^5$ cm^{-2}) none of them is satisfactory or able to account for the significant slow-down in tangle growth rate as the steady state is approached. We claim, however, that agreement with theory is recovered if the geometrical parameter c_2 introduced in numerical studies by K. W. Schwarz [Phys. Rev. B **38**, 2398 (1988)] is allowed to vary with vortex line density which also greatly improves the prediction of the observed early decay rate.

DOI: 10.1103/PhysRevB.97.064507

I. PREFACE

Thermal counterflow of superfluid ^{4}He represents the first and most extensively studied form of quantum turbulence [1–3]. Despite that, a number of open problems and unanswered questions remain that ought to be tackled both theoretically and experimentally, such as the existence and role of large vortical structures and their visualization [4–7], forms and interplay of energy spectra [8–12] in the superfluid and normal components constituting at finite temperature the superfluid ^{4}He and appropriate boundary conditions [13] for their velocity fields, small-scale universality [14], or possible relations between classical and quantum convective heat transport [15].

Recently an intense theoretical debate has arisen about what form, if any, of the so-called Vinen equation accurately captures the dynamics of vortex line density (VLD) [16–18], which motivates us to tackle this problem experimentally. Using a purposefully designed flow channel where counterflow is repeatedly generated by rectangular heat pulses and probed by second-sound attenuation we demonstrate that experimental approach is fruitful. Indeed, we find that for relatively dilute vortex tangles all proposed forms of the Vinen equation [16,19] provide adequate descriptions of its growth rate, while for dense tangles they fail and cannot account for the significant slow-down in tangle growth rate as the steady state is approached. We report data analysis that shows the way to resolve this problem, by allowing the geometrical coefficient, introduced in the theory of Schwarz [20], connecting rms curvature of quantized vortices and VLD, to depend on the VLD. Surprisingly, the observed decay rate occurring after switching off the heat is then predicted well by the observed turbulence growth rate.

The paper is organized as follows: After the introduction, Sec. II, we in Sec. III describe our experimental arrangement and in Sec. IV we present our experimental results and discuss the dynamics of the vortex tangle based on the phase portrait using a coordinate system motivated by the general form of the governing dynamical equation, prior to drawing conclusions in the last section.

II. INTRODUCTION

Normal liquid ^{4}He (He I), when cooled below the $T_\lambda \simeq 2.17$ K, undergoes a second-order phase transition; the low-temperature phase is known as He II. The physical properties of He II cannot be described by classical physics; it is a quantum fluid displaying extraordinary physical properties such as superfluidity and the two-fluid behavior. Phenomenologically, He II is described by the two-fluid model as consisting of two components: (i) viscous normal fluid of density ρ_n, carrying all the entropy content, and (ii) inviscid superfluid of density ρ_s; the total density of He II $\rho = \rho_n + \rho_s$. While at T_λ He II is entirely normal, in the zero-temperature limit there is no normal fluid; for many practical purposes He II can be thought of as entirely superfluid below about 1 K. In the limit of low velocities, He II supports two independent velocity fields $\mathbf{v}_n(\mathbf{r},t)$ and $\mathbf{v}_s(\mathbf{r},t)$; both components can easily become turbulent. Due to quantum-mechanical restrictions the otherwise potential flow of the superfluid component is violated on line singularities—cores of singly quantized vortices. Superfluid turbulence, i.e., turbulence in the superfluid component, therefore consists of a tangle of vortices carrying a single circulation quantum $\kappa \approx 9.97 \times 10^{-8}$ m^2/s each.

Quantum turbulence [3,21], defined as turbulence in quantum fluids displaying superfluidity, was first considered as a theoretical possibility by Feynman [22] and experimentally studied and theoretically described by Vinen [19,23–25] in

a peculiar thermally induced flow of He II called thermal counterflow, which can be easily set up by applying a voltage to a resistor (heater) located at the closed end of a channel of cross-section area A open to a helium bath at the other end. The heat flux $\dot{Q}$ is carried away (mean velocity v_n) from the heater by the normal fluid alone, and, by conservation of mass, i.e., $v_n\rho_n + v_s\rho_s = 0$, a superfluid current (mean velocity v_s) arises in the opposite direction. In this way a relative (counterflow) velocity $v_{ns} = |v_n| + |v_s|$, proportional to the applied heat flux, is created along the channel. Upon exceeding a critical value of v_{ns}, extrinsic vortex nucleation originating from the always present remnant vorticity leads to creation of a vortex tangle—superfluid turbulence in the superfluid component of He II.

Vinen introduced for the description of counterflow turbulence a phenomenological model based on the concept of a random vortex tangle characterized by the approximately homogeneous VLD, L. Apart from the size of the vortex core $\xi \cong 10^{-10}$ m, there is only one characteristic length scale: the quantum length scale $\delta \cong L^{-1/2}$, the mean distance between quantized vortices in the tangle. He argued that L (which is a measurable quantity with the dimensions of length per volume) obeys the equation of general form

$$\frac{dL}{dt} = F(L; v_{ns}) = \left(\frac{\partial L}{\partial t}\right)_{prod} - \left(\frac{\partial L}{\partial t}\right)_{dec}; \qquad (1)$$

i.e., the dynamics of VLD is understood as the interplay between two processes one of which acts to create the VLD and the other to destroy it. With the particular form of the production and decay terms this equation has been known as Vinen's equation

$$\frac{dL}{dt} = \alpha_V v_{ns} L^{3/2} - \beta_V L^2, \qquad (2)$$

where α_V and β_V are parameters, α_V being proportional to the mutual friction parameter α tabulated in Ref. [26]. In his original study [19] Vinen admitted that other forms of Eq. (2) cannot be excluded and an alternative production term, quadratic in v_{ns}, has been suggested that accounted for the experimental observation with sufficient accuracy. For detailed theoretical discussion of possible forms of Eq. (1) we direct the reader to the review of Nemirovskii and Fiszdon [27].

Recently the interest in Eq. (1) describing the dynamics of L in counterflow turbulence has been renewed and resulted in an intense theoretical debate between the L'vov's group [16,17] and Nemirovskii [18]. Theoretical analysis and numerical experiments based on nonhomogeneous counterflow led Khomenko *et al.* [16] to suggested yet another form of Eq. (1) and claimed that, while satisfying the quadratic $L \propto v_{ns}^2$ relation, it better describes the numerical data for a counterflow possessing a particular artificial flow profile.

In general, the various proposed forms of the Vinen equation can be written as

$$\frac{dL}{dt} = C_n v_{ns}^n L^{2-n/2} - D_n L^2, \qquad (3)$$

where $n = 1,2$ for the original or alternative Vinen equation and $n = 3$ for the equation of Khomenko *et al.* [16], and C_n, D_n are adjustable parameters suitable for the given model. For steady state, the equation of the form of Eq. (3) predicts that $L \propto v_{ns}^2$ regardless of the exponent n. This relation has been experimentally verified many times not only for counterflow turbulence (see reviews [27,28] and references to original papers therein), but more recently also for steady state of pure superflow in relatively wide channels with ends blocked by superleaks allowing the net through-flow of the superfluid component only [29].

The first theory which attempted to connect microscopic equations of motion of a quantized vortex with the dynamics of VLD is that of Schwarz [20,30]. It is based on the mesoscopic picture of superfluid turbulence developed by him—the vortex filament model [20,30,31], describing the quantized vortices as infinitesimally thin lines with no internal structure. This model led to successful pioneering numerical simulations (which were later significantly advanced by several groups [32–34]) of quantum turbulence and is still in common use today [35]. In the so-called local induction approximation (LIA)—an approximation where the long-range interaction between the vortices is ignored—the model leads to an analytical prediction of the dynamical equation [20]

$$\frac{dL}{dt} = \alpha I_l v_{ns} L^{3/2} - \beta\alpha c_2^2 L^2, \qquad (4)$$

where

$$\beta = \frac{\kappa}{4\pi}\ln\left(\frac{1}{c_1 L^{1/2}\xi}\right), \qquad (5)$$

with ξ the vortex core size, I_l one of the anisotropy indices introduced by Schwarz [20], and c_1, c_2 the geometrical coefficients connecting the mean $\bar{S}$ or rms $\tilde{S}$ curvature of the vortices in the tangle with the VLD: $\bar{S} = c_1 L^{1/2}$, $\tilde{S} = c_2 L^{1/2}$. It should be noted that recent analysis [17,36] of a general inhomogeneous counterflow in the framework of the vortex filament model suggests that the situation might be more complicated, with closures being necessary for new separate fields of anisotropy or the curvature. In particular, even though Eq. (4), as written, suggests that $n = 1$, the closure necessary for, say, I_l might change this. For completeness we note that, formally, Eq. (3) with $n = 1$ coincides with Eq. (4) for $C_1 = \alpha I_l$ and $D_1 = \beta\alpha c_2^2$.

Several experimental works in the past have studied the dynamics of VLD in (particularly free) decay of thermal counterflow. These studies are complicated by the appearance of nonmonotonic behavior (commonly called a "bump"). This feature is presently outside the scope of this article, but is thought to be connected with the redistribution of energy across scales in the coupled system of normal fluid turbulence and the vortex tangle and the formation of classical energy cascade observed in late decay [9,10].

We believe that from the point of view of the intrinsic tangle dynamics a more suitable approach is to study transitions between two turbulent states, especially the growth part. Growth of VLD in a previously quiescent helium can go through complex evolution probably connected to sudden advection of remnant vorticies pinned to the wall [37]. Additionally, growth from nonzero VLD does not seem to exhibit the nonmonotonic behavior common in the decay. Lastly, the theories of VLD dynamics should work equally well in the turbulence growth but have received little testing in this regime [38]. Following Schwarz and Rozen [38], our goal is therefore to experimen-

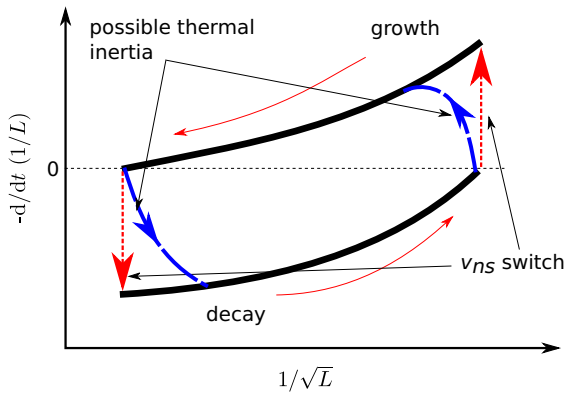

FIG. 1. Idealized sketch of the phase portrait of VLD according to Eq. (6) for sharp changes in the heat flux. See Sec. III for the explanation of the indicated possible thermal inertia.

tally test the proposed models of the dynamics of VLD using transients between two well-defined turbulent states of thermal counterflow, with the emphasis on the growth of turbulence.

In order to study the dynamics, one can compare the experimentally observed time evolution of $L(t)$ with the solution of the appropriate differential equation. The solutions to the proposed Eq. (3) are, however, very similar and difficult to distinguish. Plus, this path *a priori* restricts the possible functional forms of F in Eq. (1) with little justification. A more direct way of studying the dynamics is to look at the phase portrait (i.e., a set of trajectories in the phase space) of $L(t)$. A straightforward choice of phase space would be (L, $\dot{L}$), where the dot denotes differentiation with respect to time. However, a slight manipulation of Eq. (3) gives us a much simpler expression on the right-hand side:

$$-\frac{d}{dt}\left(\frac{1}{\ell}\right) = L_0 D_n\left[\left(\frac{1}{\sqrt{\ell}}\right)^n - 1\right], \tag{6}$$

where $\ell(t) = L(t)/L_0$ is a dimensionless VLD and $L_0 = (C_n/D_n)^{n/2}\, v_{\rm ns}^2$ is the steady-state VLD corresponding to the instantaneous counterflow velocity $v_{\rm ns}$. Motivated by this simple functional form we chose to work with the phase space $(\frac{1}{\sqrt{\ell}}, -\frac{d}{dt}(\frac{1}{\ell}))$. The physical meaning of these axes is the rate of change of the average (dimensionless) area occupied by a vortex (intervortex spacing squared) as a function of (dimensionless) intervortex spacing. The Schwarz equation, Eq. (4), in these variables reads

$$-\frac{d}{dt}\left(\frac{1}{\ell}\right) = \alpha\beta c_2^2 L_0\left(\frac{1}{\sqrt{\ell}} - 1\right). \tag{7}$$

An expected form of a phase trajectory of VLD according to Eq. (6) or (7) for sharply switching counterflow velocity between two turbulent steady states is sketched in Fig. 1.

Note that the dimensionless VLD defined as $\ell = L/L_0$ is unsuitable for free decay due to the fact that $L_0 = 0$. For decays we therefore define the dimensionless VLD: $\tilde{\ell} = L/L_i$ where L_i is the initial VLD from which the decay starts. This definition leads to only a small modification of Eq. (6)

$$-\frac{d}{dt}\left(\frac{1}{\tilde{\ell}}\right) = L_0 D_n\left[\left(\frac{v_{\rm ns}}{v_{\rm ns}^{\rm i}}\right)^n\left(\frac{1}{\sqrt{\tilde{\ell}}}\right)^n - 1\right], \tag{8}$$

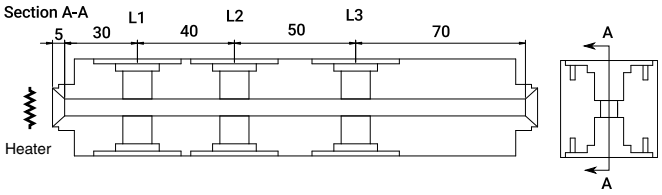

FIG. 2. A sketch of the geometrical arrangement of the channel. The figure is to scale. The counterflow is created by a resistive heater placed at one end of the channel (left end of the channel in the figure). The channel is positioned vertically, with the heater at the bottom, and placed in a bath cryostat. The heater is approximately 1 cm from the channel entrance inside a detachable small brass enclosure which is connected to the main channel cavity and sealed against the bath through an indium o-ring.

where $v_{\rm ns}$ is the instantaneous counterflow velocity and $v_{\rm ns}^{\rm i}$ is the one that produced $L_{\rm i}$. In a similar way, Eq. (7) becomes

$$-\frac{d}{dt}\left(\frac{1}{\tilde{\ell}}\right) = \alpha\beta c_2^2 L_0\left(\frac{v_{\rm ns}}{v_{\rm ns}^{\rm i}}\frac{1}{\sqrt{\tilde{\ell}}} - 1\right). \tag{9}$$

In the following we drop the $\tilde{\ell}$ notation because dimensionless growth and decay curves are never shown together.

III. EXPERIMENTAL ARRANGEMENT

The counterflow turbulence we study is set up in a brass channel of square cross section $A = 7 \times 7$ mm^2 sketched in Fig. 2. The channel length is approximately 21 cm. The counterflow is generated using a resistive heater of about 50 Ω. During the experiments the temperature of the bath is controlled within 0.1 mK by pumping rate of the bath in combination with temperature controller; for further experimental details, see our previous reports [29,39].

In order to study the dynamics of VLD with the aforementioned methods, some sort of nonstationarity is necessary. Additionally, the numerical differentiation of experimental data requires strong reduction of experimental noise. We achieve both of these goals by modulating the counterflow velocity in a channel by a square wave; see Fig. 6. We measure several thousands of transients which, when averaged, provide us with sufficiently low noise data sets to allow for numerical differentiation. The differentiation is performed either using centered differences or using a weakly smoothing cubic spline. Both methods gave nearly identical results, the only difference being slightly larger noise with the centered differences. Spline differentiation was used for all data shown in this paper.

Since the problem under study represents a strongly nonstationary flow, thorough understanding of all physical processes triggered in the channel by switching on and off the applied heat flux is necessary. Not all of these processes are necessarily directly related to the dynamics of the turbulent tangle of quantized vortices. It is useful to describe these processes by their characteristic times, which can be estimated as follows:

(1) *Kinetic characteristic time.* In steady-state counterflow in a channel $L_{\rm ch}$ long, both the normal and superfluid components of He II move, carrying kinetic energy. Neglecting the flow generated in the bath outside the channel and the turbulent velocity inside the channel, it takes time $t_{\rm char}^{\rm kin}$ to gain this kinetic

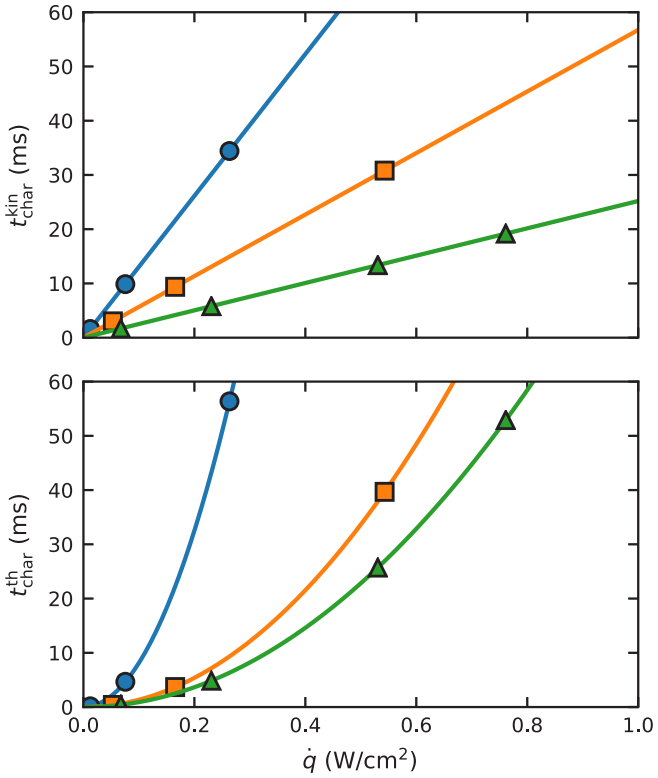

FIG. 3. Kinetic (top panel) and thermal (bottom panel) characteristic time scales given by Eqs. (11) and (13), respectively. Dependencies for the three experimental temperatures 1.45, 1.65, and 1.95 K are shown. The symbols indicate configurations where experiments took place. ●, 1.45 K; ■, 1.65 K; ▲, 1.95 K. The time constants have been calculated for the highest heat flux in a given experimental configuration. The highest point on a given curve corresponds to the last point in Table I.

energy from the heater, which can be estimated from the energy balance as

$$\dot{Q}t^{\rm kin}_{\rm char} = \rho_{\rm s} A L_{\rm ch} \frac{v_{\rm s}^2}{2} + \rho_{\rm n} A L_{\rm ch} \frac{v_{\rm n}^2}{2}. \tag{10}$$

Taking into account that in counterflow $v_{\rm s} = (\rho_{\rm n}/\rho_{\rm s})v_{\rm n}$ and $v_{\rm n} = \dot{q}/(\rho\sigma T)$, where $\dot{q} = \dot{Q}/A$ and σ denotes the entropy of He II at temperature T, we estimate the kinetic characteristic time as

$$t^{\rm kin}_{\rm char} = \frac{\rho_{\rm n}}{2\rho_{\rm s}\rho\sigma^2 T^2} L_{\rm ch}\dot{q}. \tag{11}$$

Figure 3 shows $t^{\rm kin}_{\rm char}$ for our channel for various applied heat fluxes at different temperatures.

(2) *Thermal characteristic time.* This can be estimated in the same way as in our earlier work [40]. Let us consider a switch of the applied heat input to the channel heater from $\dot{q}_1$ to $\dot{q}_2$. For simplicity, we assume linear temperature gradients in steady states, ∇T_1 and ∇T_2, leading to temperature differences $\Delta T_1 = L_{\rm ch}\nabla T_1$ and $\Delta T_2 = L_{\rm ch}\nabla T_2$, while the temperature of the helium bath, T, remains unchanged. In a steady-state counterflow, it is an established experimental fact that, for high enough VLD, $\dot{q}_1 = \zeta(T)\nabla T_1^{1/3}$, where for any temperature [19] $\zeta \simeq$ constant. On the other hand, the heat that must be either taken away or supplied between the two steady

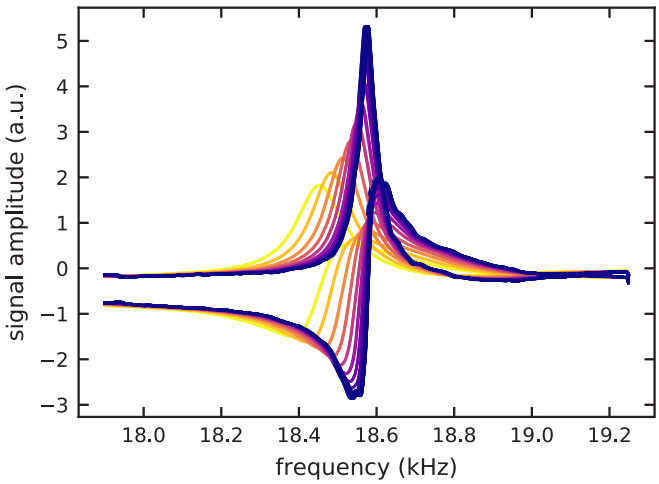

FIG. 4. Second-sound resonance peak for different counterflow velocities at 1.95 K, measured with sensor L2.

states, assuming that specific heat of He II $c(T_2) \cong c(T_1) \cong c(T) = c$, equals $Q = \frac{1}{2}c\rho A L_{\rm ch}|\Delta T_2 - \Delta T_1|$. Differentiating with respect to time, we get

$$\dot{q} = \frac{1}{2}c\rho L_{\rm ch}\Delta\dot{T}(t) = \zeta(T)[\Delta T(t)/L_{\rm ch}]^{1/3}, \tag{12}$$

which is easy to solve by separating the variables and finally yields the thermal characteristic time

$$t^{\rm th}_{\rm char} = \frac{3c\rho\left|\Delta T_2^{2/3} - \Delta T_1^{2/3}\right|}{4\zeta} L_{\rm ch}^{4/3}. \tag{13}$$

Figure 3 shows calculated $t^{\rm th}_{\rm char}$ for all individual experimental runs discussed in this paper. Temperature in the channel was monitored using multiple independent thermometers; see Ref. [37] for details.

(3) *Second-sound response time* $t^{\rm ss}_{\rm char}$. VLD is detected by measuring the extra attenuation of second sound caused by scattering of normal-component thermal excitations by the vortex lines [19]. In this work, second sound is generated and detected simultaneously by three pairs of vibrating porous membranes located in the walls of the channel as shown in Fig. 2; the second sound travels across the channel, which acts as a resonator [29,39]. An example of the second-sound resonance being attenuated by the presence of quantum turbulence is shown in Fig. 4. The attenuated amplitude of second sound at resonance, a, is related to VLD through the equation

$$L = \frac{3\pi\rho_{\rm n}\Delta f}{\rho\alpha\kappa}\left(\frac{a_0}{a} - 1\right), \tag{14}$$

where a_0 and Δf are the amplitude and full width at half maximum of the second-sound amplitude resonant curve for quiescent helium, and α is the mutual friction coefficient [26]. Correct estimation of the resonant second-sound amplitudes a and a_0 is necessary to obtain the measurement of VLD. This is a challenge for time-resolved second-sound measurements, which are of primary interest for our purposes. The changing attenuation is accurately reflected only if the natural *second-sound response time* $t^{\rm ss}_{\rm char}$ of the second-sound resonator (on the order of the product of the time in which second sound crosses the width of the channel and the time-dependent quality factor

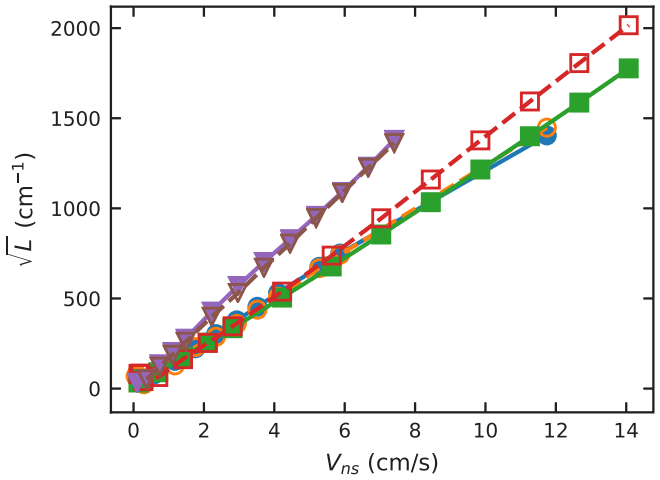

FIG. 5. Steady-state VLD as a function of the counterflow velocity. Filled symbols are measured using second-sound sensor L1, empty using sensor L2; see Fig. 2. ●, ○–1.45 K; ■, □–1.65; ▼, ▽–1.95 K.

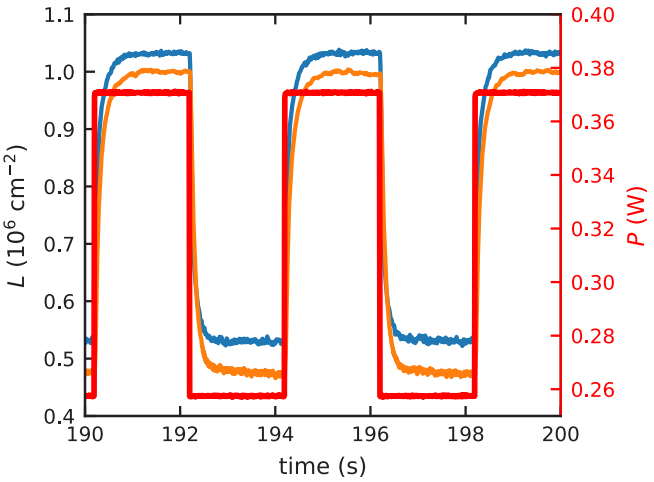

FIG. 6. Illustration of the time dependence of the VLD in modulated counterflow. The displayed case is for 1.95 K and 2 s pulse width, and modulation depth is roughly between densities of 5×10^5 and 10^6 cm^{-2}. The sharp square wave shows the time dependence of the applied heater power (with values on the right y axis). The two experimental curves show measured vortex line density with sensor L1 (higher; blue color) and L2 (lower; orange color) with values on the left y axis.

of the resonant peak) is sufficiently short—in our experiment on the order of 10 ms (for attenuated peaks). Moreover, the time-dependent measurements (such as generation and decay) are usually accomplished by tuning the excitation frequency and measuring the second-sound amplitude directly, for example as the in-phase component measured by a lock-in amplifier. This is not possible in our long channel, due to significant temperature shifts caused by the presence of the temperature gradient naturally associated with thermal counterflow. We overcome this difficulty using a postprocessing technique, described in our previous publication [37], which calculates the resonant amplitude from slightly off-resonant real and imaginary components of the complex amplitude measured with a lock-in amplifier. Another option could have been the resonance-tracking technique recently developed by Yang *et al.* [41]. We opted not to use this technique due to concerns about about resolving fast transients in a system that continually adjusts its excitation frequency.

Estimated times $t_{\rm char}^{\rm kin}$, $t_{\rm char}^{\rm th}$, and $t_{\rm char}^{\rm ss}$ are generally rather short, on the order of the time constant of the lock-in amplifier (10 ms in our case) which in turn must be chosen based on the frequency and quality factor of the second-sound resonance used for direct measurement of the VLD in the channel. The processes described above ought to work simultaneously and in parallel. The actual limitation to the experiment is therefore given roughly by the longest time constant (i.e., the slowest process) for a given experimental configuration. In our case this is always less than 60 ms—meaning that, in general, measurements of the VLD in the first 60 ms after a transient in the heat flux might be affected by processes that are not interesting from the point of view of the intrinsic tangle dynamics.

In practice, the X and Y components of all three lock-ins (for the three second-sound sensors) and the power dissipated by the counterflow heater are all sampled simultaneously by a multichannel digital-to-analog converter at a fixed rate of 100 points per second. The data measured with sensors L1 and L2 are generally very similar and the results reported below are measured with L1. Sensor L3 displayed much higher noise and was generally not used.

IV. EXPERIMENTAL RESULTS AND DISCUSSION

Vortex line density obtained in the steady state measured using the full resonance peak is shown in Fig. 5. The observed relationship between VLD and counterflow velocity obeys

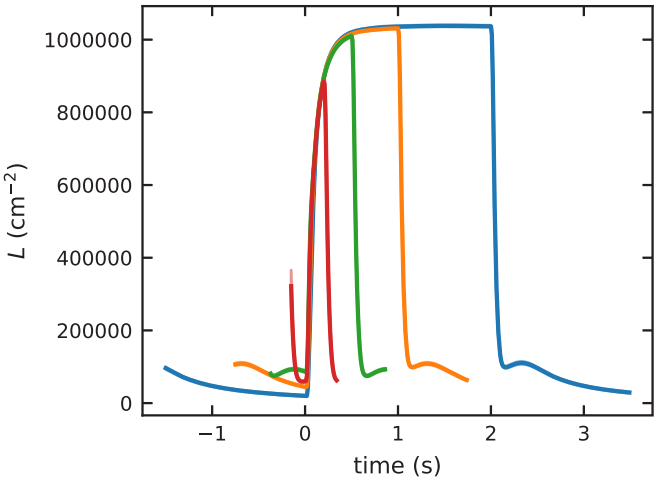

FIG. 7. Averaged growth of the VLD during a heat pulse for different pulse widths. Shown are 0.2, 0.5, 1, and 2 s pulse widths. Temperature was 1.45 K and the heat flux was pulsed between 266 mW and 0. Heat flux 266 mW corresponds to a steady-state VLD of about 10^6 cm^{-2}. The standard deviation of the average is not visible on the scale shown. The rising edge of the counterflow velocity (width of the edge of the heat flux is about 300 μs; the VLD is measured every 10 ms) is used as the time origin.

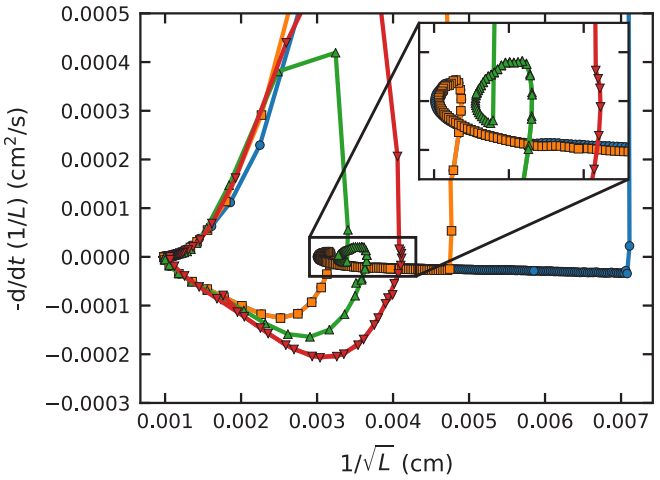

FIG. 8. Full phase portrait obtained from the pulsed heat flux. The data are the same as in Fig. 7: ●, 2 s pulse; ■, 1 s; ▲, 0.5 s; ▼, 0.2 s. The inset shows the detail of the behavior near the "bump". While the growth of the VLD is hardly affected by the pulse width, decay can be affected quite strongly.

the expected $L = \gamma^2 v_{ns}^2$ with γ coefficients approximately 129, 141, and 186 s/cm^2 for 1.45 K, 1.65 K, and 1.95 K, respectively. The values for 1.45 K and 1.65 K are within about 10% of values reported in the literature [29] whereas the 1.95 K case is either about 30% too low or within the expected range, depending on the data set with which one compares.

The dynamics of the VLD, however, cannot be studied using the properties of the steady state. In order to study the dynamical properties of the tangle we do not allow the tangle to settle to a constant value of the VLD. To achieve this in a controlled fashion we use a square-wave modulated counterflow, an example of which is shown in Fig. 6. Several thousands of the pulses have been measured and the results,

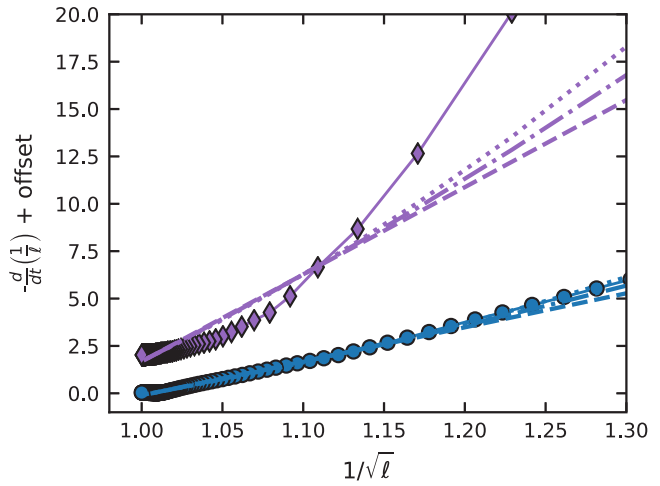

FIG. 9. Growth phase trajectory for sparse (●, modulation of VLD between 0 and 10^5 cm^{-2}) and dense (◆, modulation between 10^5 and 10^6 cm^{-2}) tangle at 1.45 K. Lines are fits of Eq. (6) with dashed line $n = 1$, dash-dotted line $n = 2$, and dotted line $n = 3$. For the sparse tangle all fits are adequate (fits for different n essentially overlap); for the dense tangle all models provide a poor description. For the fit, only $\ell \in [1, 1.2]$ are used.

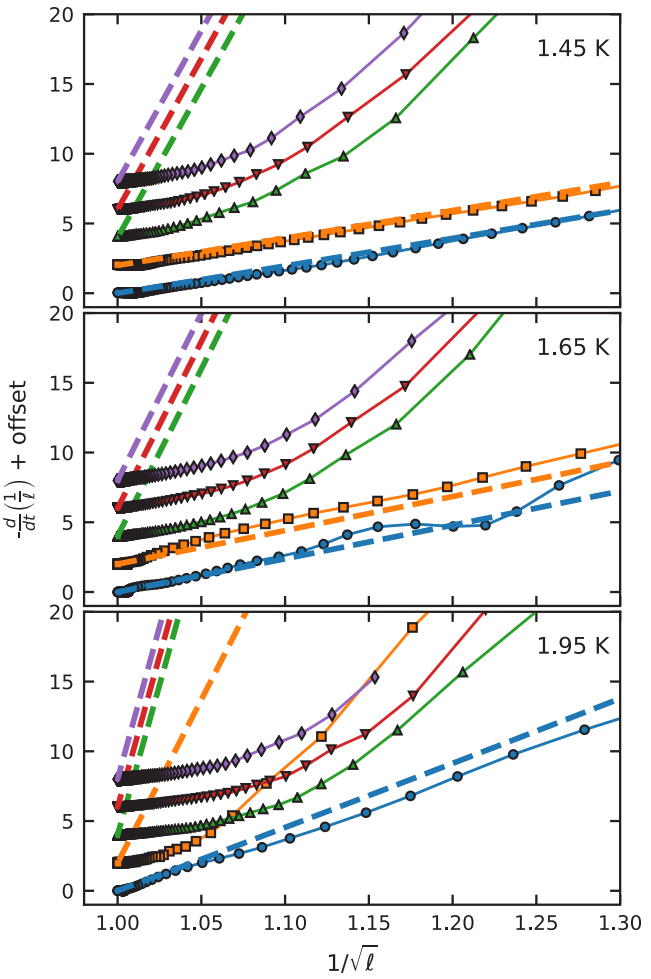

FIG. 10. Phase portrait of the VLD growth dynamics. The dashed lines coinciding with the experimental data for $1/\sqrt{\ell} = 1$ are predictions according to simulations of Schwarz [20]. The curves and the theoretical predictions are offset for clarity. We emphasize that no fitting was used in comparison of the numerical prediction with the experiment. Temperatures (top to bottom): 1.45, 1.65, and 1.95 K. VLDs high and low are increasing for the curves going from bottom to top; see Table I for details about the data sets. The y-axis offset increment is 2 in the units of the axis.

when averaged, are illustrated in Fig. 7. Attempting to fit these time dependencies using solutions to one of the expected dynamical equations bears little fruit. The solutions are, indeed, very similar and all can be said to provide an adequate fit.

In order to study the dynamics of the VLD more directly we look at its phase portrait using a coordinate system motivated by Eq. (7). A particular case for 1.45 K (the same data as in Fig. 7) and several different pulse widths is shown in Fig. 8. As can be expected already from Fig. 7, the dynamics of the VLD growth are unaffected by the pulse width; however, the decay can be quite different. The VLD alone, in general, is unsuitable for the description of the decay due to the nonmonotonic behavior usually referred to as the "bump" (seen as the small loop in the decaying part of a phase trajectory). Nonmonotonic behavior cannot be modeled by a one-dimensional dynamical system. The physical origin of the bump is beyond the scope of this article but is thought to be connected to the existence of

TABLE I. Experimental data sets shown in Figs. 10 and 12. The pulse width for the displayed cases was 2 s except for 1.45 K where it was 1 s (marked * near the symbol), 0.5 s (marked **), or 2 s for all other cases. The numbers shown are in the format $X_{\text{high}}/X_{\text{low}}$; the "high" and "low" subscripts correspond to the square-wave modulated heat flux being in the higher or lower state. For counterflow velocity v_{ns}, the average across the entire duration of the pulse is shown. For L, L_{high} is the VLD 10 ms before the heat pulse is switched to the lower state and L_{low} corresponds to to the overall minimum. Ensemble averaging is used to calculate the L_{high} and L_{low} and the standard deviation of this average is shown as the error. The two lines of the VLD correspond to second-sound sensors L1 and L2 (see Fig. 2).

Nominal VLD		1.45 K	1.65 K	1.95 K
$10^5/0$	symbol	●	●	
	v_{ns} (cm/s)	2.4/0.0	2.5/0.0	
	actual L	$79 \pm 2.7/19 \pm 2.9$	$74 \pm 3.6/7.9 \pm 2.8$	
	(10^3 cm^{-2})	$64 \pm 6.8/13 \pm 6.6$	$82 \pm 1.4/16 \pm 1.5$	
$10^5/10^4$	symbol	■	■	●
	v_{ns} (cm/s)	2.4/0.4	2.5/0.8	1.8/0.5
	actual L	$79 \pm 2.4/19 \pm 2.5$	$75 \pm 3.3/13 \pm 3.0$	$97 \pm 1.9/7.5 \pm 2.5$
	(10^3 cm^{-2})	$65 \pm 7.1/16 \pm 7.0$	$83 \pm 3.3/15 \pm 3.2$	$85 \pm 2.2/5.0 \pm 3.1$
$5 \times 10^5/10^5$	symbol			■
	v_{ns} (cm/s)			4.3/1.8
	actual L			$54 \pm 0.39/10 \pm 0.67$
	(10^4 cm^{-2})			$48 \pm 0.39/8.5 \pm 0.47$
$10^6/0$	symbol	▲**	▲	▲
	v_{ns} (cm/s)	8.4/0.0	8.3/0.0	6.1/0.0
	actual L	$97 \pm 0.47/11 \pm 0.34$	$83 \pm 0.25/1.3 \pm 0.22$	$100 \pm 0.52/1.8 \pm 0.52$
	(10^4 cm^{-2})	$96 \pm 2.4/13 \pm 0.70$	$100 \pm 0.26/2.0 \pm 0.18$	$99 \pm 0.49/1.7 \pm 0.45$
$10^6/10^4$	symbol	▼	▼	▼
	v_{ns} (cm/s)	8.4/0.4	8.3/0.8	6.1/0.5
	actual L	$99 \pm 0.82/5.7 \pm 0.34$	$83 \pm 0.34/1.5 \pm 0.28$	$100 \pm 0.42/0.61 \pm 0.47$
	(10^4 cm^{-2})	$98 \pm 2.3/6.3 \pm 0.65$	$100 \pm 0.62/0.91 \pm 0.26$	$98 \pm 0.58/0.96 \pm 0.62$
$10^6/10^5$	symbol	◆	◆	
	v_{ns} (cm/s)	8.4/2.4	8.3/2.5	
	actual L	$99 \pm 0.48/9.2 \pm 0.21$	$83 \pm 0.20/7.6 \pm 0.13$	
	(10^4 cm^{-2})	$98 \pm 2.4/8.7 \pm 0.63$	$100 \pm 0.37/7.3 \pm 0.20$	
$10^6/5 \times 10^5$	symbol			◆
	v_{ns} (cm/s)			6.1/4.3
	actual L			$100 \pm 0.35/53 \pm 0.43$
	(10^4 cm^{-2})			$100 \pm 0.73/48 \pm 0.64$

energy at large scales in quantum turbulence [9,10]. Note that the VLD is sampled at a rate of 100 points/s; i.e., all points are equidistant in time and separated by 10 ms. The first five or six points after a transient might be affected by parasitic effects; see Sec. III. From now on, the first 50 ms of the growth phase trajectories are never shown. Decay trajectories will be shown in full.

Looking at the phase trajectories of two particular cases of high and low VLD transients from 1.45 K in Fig. 9 we immediately see that trying to decide between the different forms of the Vinen equation Eq. (3), in particular which exponent from the three proposed models of $n = 1,2,3$ best describes the data, is an ill-posed question. The behavior of these functions is very similar and for sparse tangles the fits are adequate regardless of the exponent. For dense tangles, none of the models provides a good description. In the following, we chose to base most of our interpretation on the model of Schwarz (and assuming that $n = 1$) since that is the simplest currently available theory that connects the microscopic physics of the motion of the vortices with macroscopic VLD dynamics.

The growth part of the phase portrait for different modulated flows is shown in Fig. 10 (see Table I for classification of all data sets in Fig. 10). As a point of reference, we compare our experimental data with numerical simulations obtained by Schwarz [20] expressed through Eq. (7). The numerical values of the coefficient c_2 for the experimental temperatures have been obtained by cubic spline interpolation of the data published in Ref. [20]. We observe that the agreement between the experimental data and simulations, with no adjustable parameters, is nearly perfect for tangles with relatively low VLD. The measured approach to the steady state, however, is significantly less steep for dense tangles. As a way to capture this behavior quantitatively we allow the geometric coefficient c_2 to vary with VLD. The c_2 coefficient as a function of intervortex distance obtained from these growth curves is shown in Fig. 11. A sharp increase in c_2 is seen for the 1.65 K and, to a lesser extent, for 1.95 K, for small tangle densities. For these cases, small oscillations in L are observed (visible also in Fig. 10), especially early after the transient (not shown in Fig 10), probably related to temperature instability and nonideal second-sound resonance. In the first 50 ms after the transient (which are not used for analysis; these points are not shown) a sharp swing to smaller c_2 is seen. Therefore we regard these points as experimental artifacts [43]. It should also

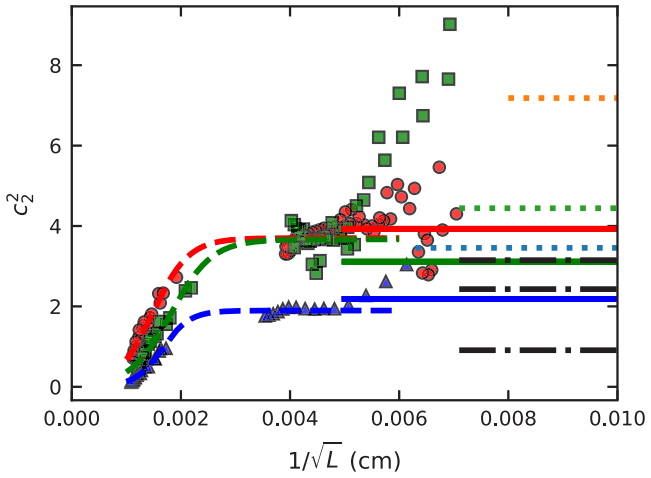

FIG. 11. Effective coefficients c_2 as a function of the mean intervortex distance. ●, 1.45 K; ■, 1.65 K; ▲, 1.95 K. The horizontal full lines show c_2 interpolated for experimental temperatures from values calculated by Schwarz [20] corresponding to 1.45, 1.65, and 1.95 K (top to bottom). The dashed lines are least squares fits to Eq. (15). Black dash-dotted lines on the right: numerical simulations of a vortex tangle with uniform normal fluid, synthetic turbulence, and frozen Navier-Stokes turbulence in normal fluid, respectively from top to bottom, from Ref. [42]. See text for estimation of c_2 from average curvature. Dotted lines on the right: c_2 from Ref. [34] for 1.3 K, 1.6 K, and 1.9 K (top to bottom). Lines from Ref. [42] and Ref. [34] terminate at the minimum intervortex distance that these simulations achieved (except for the top dashed 1.3 K case, where the intervortex spacing was 125 μm). The tendency of the experimental points to rise for small vortex line densities is most likely an experimental artifact; see text for discussion.

be noted that for simplicity, we neglected the changes in c_1 in the logarithmic correction given by Eq. (5) and simply used the values obtained by Schawrz [20,44]

Physically, it is tempting to keep the original interpretation of c_2 as a way to measure the rms curvature of the tangle. However, the dynamical equation that leads to the calculation of c_2 from the experimental data was an approximation for relatively sparse tangles (so that the local-induction approximation is sufficient) and for only quasistationary processes. It should be noted though that systematic numerical studies [34] have shown that scaling of tangle rms curvature with the VLD remains valid even when the nonlocal full Biot-Savart interaction is taken into account. These simulations yielded c_2's which are somewhat higher than those predicted by [20] but roughly within the range of the experimental values, except for their lowest 1.3 K. The comparison with c_2's from [34] (average of values for different reconnecting algorithms) is shown in Fig. 11. No decrease of c_2 with increasing VLD has been observed in simulations of steady-state counterflow with uniform normal fluid velocity; however, two numerical experiments observed changes in the tangle curvature which could be said to be in agreement with our experimental findings: (i) at fairly low temperatures, Kondaurova *et al.* [45] observed that in freely decaying turbulence c_2 increases as the VLD decreases, and (ii) simulations which used quasiturbulent normal fluid velocity field [42] (either synthetic turbulence or a

TABLE II. Adjustable parameters of the expression Eq. (15) for the empirical c_2.

Temperature (K)	ϕ (cm)	ϑ (cm)	C
1.45	1.49×10^{-3}	6.54×10^{-4}	1.85
1.65	1.82×10^{-3}	7.46×10^{-4}	1.83
1.95	1.66×10^{-3}	5.03×10^{-4}	0.95

stationary "frozen" snapshot of a DNS simulation of classical turbulence at one temperature 1.95 K and one steady VLD of about 2×10^4 cm^{-2}) have demonstrated marked decrease in average curvature compared to the uniform case. Data in [42] are reported in terms of mean curvature $\bar{S}$. In order to transform them to rms curvature $\tilde{S}$ we use the estimate of Kondaurova *et al.* [34] $\tilde{S} = \bar{S}\sqrt{3/2}$ which is then used to calculate c_2 using the reported VLD. The result is also shown in Fig. 11. If we were to take the decrease in c_2 as an empirical fact, it would be an interesting question whether the main cause is the normal fluid turbulence or the high tangle density. One possibility of shedding some light on this issue is to repeat the experiments in a mechanically generated counterflow (pure superflow) [39], where the normal component should be on average at rest. These experiments are planned in our laboratory.

One should bear in mind that the numerical simulations can as yet achieve only relatively low VLD (on the order of 10^4 cm^{-2}, i.e., about 10 times lower than our present smallest experimental VLD), where it is challenging to obtain experimental data with sufficiently low noise to allow differentiation. In addition, the simple models Eq. (3) or (4) introduced earlier assume homogeneous counterflow and an unbound system (although there have been fruitful attempts [16,36] to capture inhomogeneity by introducing a flux term in the dynamical equation). Thermal counterflow is known to be somewhat inhomogeneous, both from experiments [7] and simulations [46], especially at relatively low counterflow velocities in wall-bounded setups. However, the inhomogeneous turbulence observed in Ref. [7] referred to a low-velocity state (less than about 0.8 cm/s in their system), whereas for the velocities more typically used in our experiments mostly statistically homogeneous turbulence in the normal fluid was observed. Furthermore, the curvature in Ref. [46], except for very near the wall, was observed to be almost homogeneous. Lastly, in our reported tangles the typical intervortex spacing is 0.01–0.1 mm (0.01–0.03 mm for the more dense states), which, even in the worst case, is separated from the size of the system (7 mm) by nearly two orders of magnitude. We therefore consider finite-size effects to play little role in our experimental data. It should also be noted that due to the nature of second-sound attenuation measurements, the value of the VLD measured is an average over a volume of about 0.3 cm^3 (7 mm cubed) and over a time interval of about 10 ms (the time constant of the lock-in amplifier); therefore we do not have access to local information. One way to probe tangle inhomogeneity would be to use low-lying modes of the second-sound resonator [47]; however, this was not possible in the current work and all the resonances used were higher than the 10th harmonic, which measures the VLD uniformly across the channel.

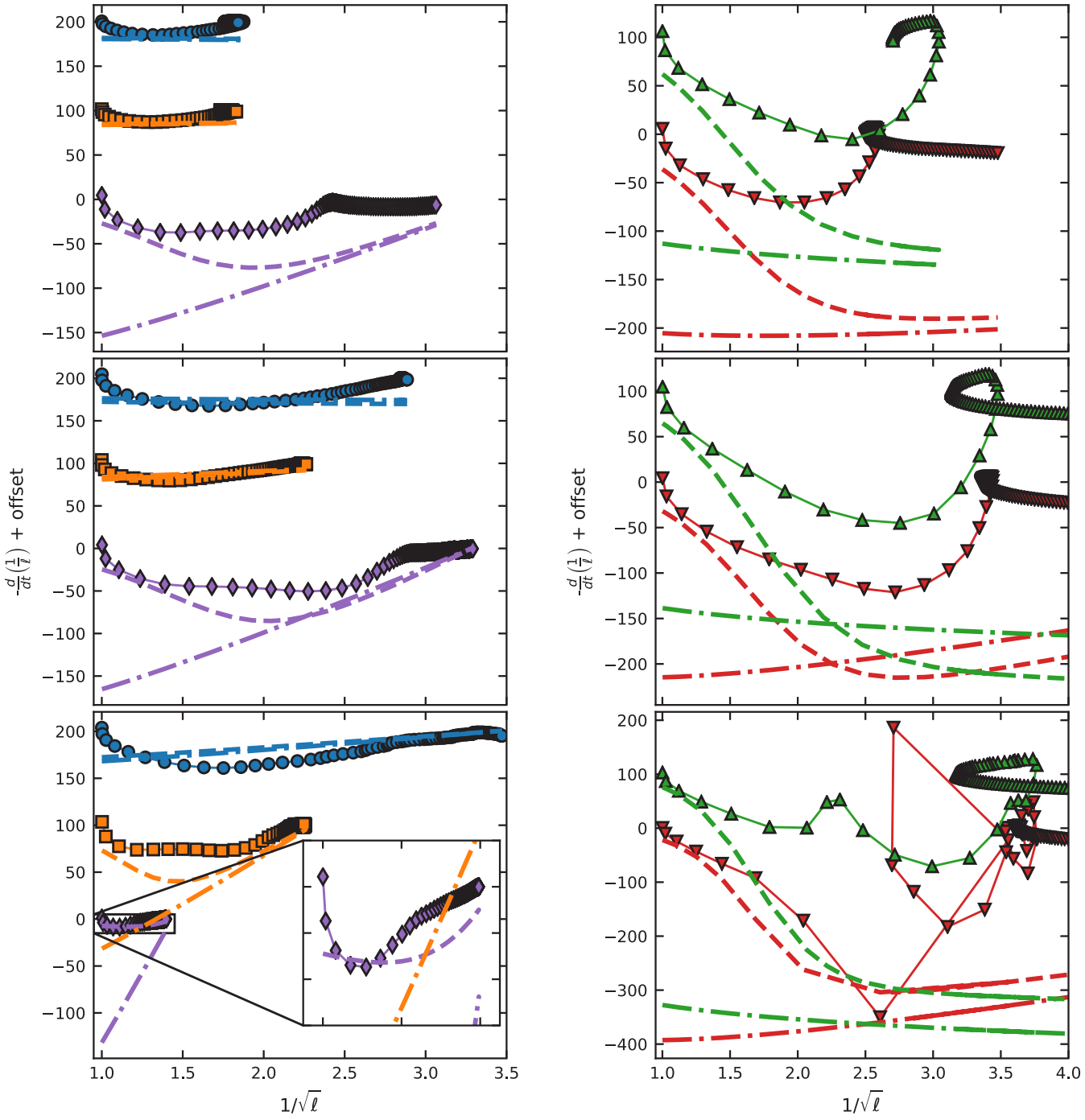

FIG. 12. Phase portrait of the decaying turbulence. Shown with the data are also theoretical predictions using c_2 coefficients either from Schwarz [20] (dash-dotted lines) or obtained from the fit of the experimental data (dashed lines). Temperatures are (top to bottom) 1.45 K, 1.65 K, and 1.95 K. The y-axis offset increment is 100 in the units of the axis. List of shown data sets is in Table I. Left: Smaller transients for which nominal $L_{\rm high}/L_{\rm low} \leqslant 100$ or $L_{\rm high} = 10^5$ cm^{-2}. Right: Larger transients for which nominal $L_{\rm high}/L_{\rm low} \geqslant 100$ and $L_{\rm high} = 10^6$ cm^{-2}. For 1.95 K, very early after switching the heat flux, it is very challenging to compensate for the resulting shifts in the second-sound resonance, hence the disruptions in the decay curves; see the shift in Fig. 4.

For simplicity of handling the empirical c_2 in the subsequent analysis we approximate the experimental data with a simple formula

$$c_2^2(\delta) = C\left[1 + \tanh\left(\frac{\delta - \phi}{\vartheta}\right)\right], \qquad (15)$$

where $\delta = 1/\sqrt{L}$ is the intervortex spacing and C, ϕ, ϑ are adjustable parameters. The reason for this particular functional form is simply convenience and the fact that $c_2^2 > 0$ by definition. The function parameters obtained by nonlinear least squares fitting are given in Table II.

Even though we *a priori* accept that the VLD dynamical equations are in general unsuitable for the description of

the decay, it is interesting to compare the phase trajectory of the decaying turbulence with the prediction based on the dynamical equation; see Fig. 12. Using the c_2 coefficients calculated by Schwarz (dot-dashed lines) we obtain reasonable agreement in decay rate for sparse tangles but a very gross mismatch for denser tangles, where the actual decay rate is much smaller (in absolute value) than predicted. However, using the (variable) empirical c_2 coefficients obtained from the growth brings the decay rate much closer to reality and even reproduces some qualitative features. Agreement is good even for the very dense tangles and becomes worse only for the free (no residual v_{ns}) or nearly free (small residual v_{ns}) decay from very high density. Moreover, the initial decay rate for all tangles is estimated to a high degree of accuracy. The slow initial decay rate has usually been explained using the residual heat flux due to thermal RC time constant [i.e., Eq. (13)]. These results suggest that the importance of the thermal time constant for the tangle dynamics may have been overstated.

V. CONCLUSIONS

The vortex tangle in quantum turbulence is a very complex system and as such vortex line density, and its dynamics, alone provide only a very coarse description. However, due to the simplicity and time-tested reliability of second-sound measurements and the existence of relatively simple theories of VLD dynamics in a homogeneous counterflow it is important to establish the boundaries within which the description of superfluid turbulence using just the VLD is sufficient, how, if at all, the straightforward ideas about tangle motions relate to the experimental reality, and in what way the line-density-centric description of quantum turbulence breaks down.

With these goals in mind we studied thermal counterflow in a channel in a situation where the turbulence is not allowed to settle, in a controlled way, to a statistical steady state. This we achieved by modulating the counterflow velocity in the channel by a square wave. The large number of turbulent transients thus obtained allows us not only to study the time evolution of the VLD but also to focus on the dynamics of the VLD more directly using its phase portrait, a common tool for studying dynamical systems.

We find that for small overall tangle densities all proposed forms of Eq. (3) provide adequate description. For higher densities, across all temperatures, these forms of the dynamical equation cannot account for the significant slow-down in tangle growth rate as the steady state is approached (Fig. 10). A possible approach to the description of this problem is to allow the geometrical coefficient c_2, connecting rms curvature of quantized vortices and the VLD, to depend on the VLD. Calculating c_2 using the theory of Schwarz [20], Eq. (7), we find (see Fig. 11) that c_2 is close to the value expected from numerical simulations for relatively sparse tangles but decreases markedly for densities $L > 5 \times 10^5$ cm^{-2}. This is also in accord with the observed decrease in curvature, which was found in numerical simulations of thermal counterflow in the presence of classical turbulence in the normal fluid [42].

An important and striking observation is that even for large counterflow velocities and dense tangles, where the phase portrait does not have a form predicted by Eq. (6), the decay rate occurring after the falling edge of the heat flux is predicted well by the turbulence growth by using the effective estimated parameter c_2, as shown in Fig. 12.

It is our hope that we have demonstrated the utility and power of looking at the behavior of the VLD from the point of view of dynamical systems. Specifically, second-sound measurements of the growth of turbulence might provide us with a way to measure mean curvature of the tangle. The observed dynamics are complex, but we believe that further study following this line could provide deeper understanding of the tangle dynamics even in highly turbulent cases. More measurements, especially at higher temperatures closer to the lambda point and other types of quantum flows, are, however, clearly needed.

ACKNOWLEDGMENTS

We thank M. J. Jackson, M. La Mantia, V. S. L'vov, A. Pomyalov, D. Schmoranzer, F. Soukup, P. Švančara, and W. F. Vinen for fruitful discussions, and L. Doležal for skillful manufacturing of the counterflow channel. This research is funded by the Czech Science Foundation under project GAČR 17-03572S. E.V. acknowledges support from the Charles University under GAUK 368217.

[1] W. F. Vinen and J. J. Niemela, J. Low Temp. Phys. **128**, 167 (2002).
[2] L. Skrbek and K. R. Sreenivasan, Phys. Fluids **24**, 011301 (2012).
[3] C. F. Barenghi, L. Skrbek, and K. R. Sreenivasan, Proc. Natl. Acad. Sci. USA **111**, 4647 (2014).
[4] M. S. Paoletti, M. E. Fisher, K. R. Sreenivasan, and D. P. Lathrop, Phys. Rev. Lett. **101**, 154501 (2008).
[5] W. Guo, M. La Mantia, D. P. Lathrop, and S. W. Van Sciver, Proc. Natl. Acad. Sci. USA **111**, 4653 (2014).
[6] M. La Mantia and L. Skrbek, Phys. Rev. B **90**, 014519 (2014).
[7] A. Marakov, J. Gao, W. Guo, S. W. Van Sciver, G. G. Ihas, D. N. McKinsey, and W. F. Vinen, Phys. Rev. B **91**, 094503 (2015).
[8] A. W. Baggaley, C. F. Barenghi, and Y. A. Sergeev, Phys. Rev. B **85**, 060501 (2012).
[9] J. Gao, W. Guo, V. S. L'vov, A. Pomyalov, L. Skrbek, E. Varga, and W. F. Vinen, JETP Lett. **103**, 648 (2016).
[10] S. Babuin, V. S. L'vov, A. Pomyalov, L. Skrbek, and E. Varga, Phys. Rev. B **94**, 174504 (2016).
[11] J. Gao, E. Varga, W. Guo, and W. F. Vinen, Phys. Rev. B **96**, 094511 (2017).
[12] M. Tsubota, K. Fujimoto, and S. Yui, J. Low Temp. Phys. **188**, 119 (2017).
[13] G. W. Stagg, N. G. Parker, and C. F. Barenghi, Phys. Rev. Lett. **118**, 135301 (2017).
[14] M. La Mantia, P. Švančara, D. Duda, and L. Skrbek, Phys. Rev. B **94**, 184512 (2016).

[15] L. Skrbek, A. V. Gordeev, and F. Soukup, Phys. Rev. E **67**, 047302 (2003).
[16] D. Khomenko, L. Kondaurova, V. S. L'vov, P. Mishra, A. Pomyalov, and I. Procaccia, Phys. Rev. B **91**, 180504 (2015).
[17] D. Khomenko, V. S. L'vov, A. Pomyalov, and I. Procaccia, Phys. Rev. B **94**, 146502 (2016).
[18] S. K. Nemirovskii, Phys. Rev. B **94**, 146501 (2016).
[19] W. F. Vinen, Proc. R. Soc. A Math. Phys. Eng. Sci. **242**, 493 (1957).
[20] K. W. Schwarz, Phys. Rev. B **38**, 2398 (1988).
[21] The term "quantum turbulence" was introduced into the literature by R. J. Donnelly in a symposium dedicated to the memory of G. I. Taylor; see Ref. [48].
[22] R. P. Feynman, Prog. Low Temp. Phys. **1**, 17 (1955).
[23] W. F. Vinen, Proc. R. Soc. A Math. Phys. Eng. Sci. **240**, 114 (1957).
[24] W. F. Vinen, Proc. R. Soc. A Math. Phys. Eng. Sci. **240**, 128 (1957).
[25] W. F. Vinen, Proc. R. Soc. A Math. Phys. Eng. Sci. **243**, 400 (1958).
[26] R. J. Donnelly and C. F. Barenghi, J. Phys. Chem. Ref. Data **27**, 1217 (1998).
[27] S. K. Nemirovskii and W. Fiszdon, Rev. Mod. Phys. **67**, 37 (1995).
[28] J. T. Tough, Prog. Low Temp. Phys. **8**, 133 (1982).
[29] S. Babuin, M. Stammeier, E. Varga, M. Rotter, and L. Skrbek, Phys. Rev. B **86**, 134515 (2012).
[30] K. W. Schwarz, Phys. Rev. B **31**, 5782 (1985).
[31] K. W. Schwarz, Phys. Rev. Lett. **49**, 283 (1982).
[32] H. Adachi, S. Fujiyama, and M. Tsubota, Phys. Rev. B **81**, 104511 (2010).
[33] A. W. Baggaley and C. F. Barenghi, J. Low Temp. Phys. **166**, 3 (2012).
[34] L. Kondaurova, V. S. L'vov, A. Pomyalov, and I. Procaccia, Phys. Rev. B **89**, 014502 (2014).
[35] R. Hanninen and A. Baggaley, Proc. Natl. Acad. Sci. USA **111**, 4667 (2014).
[36] D. Khomenko, V. S. L'vov, A. Pomyalov, and I. Procaccia, Phys. Rev. B **97**, 014508 (2018).
[37] E. Varga, S. Babuin, V. S. L'vov, A. Pomyalov, and L. Skrbek, J. Low Temp. Phys. **187**, 531 (2017).
[38] K. W. Schwarz and J. R. Rozen, Phys. Rev. B **44**, 7563 (1991).
[39] S. Babuin, E. Varga, W. F. Vinen, and L. Skrbek, Phys. Rev. B **92**, 184503 (2015).
[40] A. Gordeev, T. Chagovets, F. Soukup, and L. Skrbek, J. Low Temp. Phys. **138**, 549 (2005).
[41] J. Yang, G. G. Ihas, and D. Ekdahl, Rev. Sci. Instrum. **88**, 104705 (2017).
[42] L. K. Sherwin-Robson, C. F. Barenghi, and A. W. Baggaley, Phys. Rev. B **91**, 104517 (2015).
[43] Using sensor L2 (see Fig. 2), the low-VLD c_2^2's for 1.45 K are 10%–20% higher than those measured using L1, but exhibit similar problems. For temperatures 1.65 K and 1.95 K the c_2's from sensors L1 and L2 agree within the experimental scatter.
[44] Recalculating c_2 using an order of magnitude smaller c_1 than obtained by Schwarz results in about 15% change in c_2^2, which is within the experimental scatter.
[45] L. Kondaurova, V. S. L'vov, A. Pomyalov, and I. Procaccia, Phys. Rev. B **90**, 094501 (2014).
[46] A. W. Baggaley and S. Laizet, Phys. Fluids **25**, 115101 (2013).
[47] E. Varga, S. Babuin, and L. Skrbek, Phys. Fluids **27**, 065101 (2015).
[48] R. J. Donnelly and C. E. Swanson, J. Fluid Mech. **173**, 387 (1986).